



Experiments and calculations of wave breaking and evolution of wave groups with high steepness

Wen-yang Duan, Kun Zheng, Bin-bin Zhao*

College of Shipbuilding Engineering, Harbin Engineering University, Harbin 150001, China

(Received May 8, 2022, Revised July 28, 2022, Accepted September 1, 2022, Published online September 29, 2022)
 ©China Ship Scientific Research Center 2022

Abstract: The evolution of the nonlinear wave groups in deep water is investigated through laboratory measurements and numerical analysis. Laboratory experiments are conducted in deep-water wave tank, focusing on the characteristics of breaking waves arising from the evolved wave train. Some quantitative results are obtained for the significant breaking wave train, including the surface elevation time series, the local geometry, and the energy dissipation. A nonlinear model for the evolution of the wave groups in deep water is developed by adding eddy viscosity dissipation terms in the High Level Irrotational Green-Naghdi (HLIGN) equations. The results of the simulation are compared with the laboratory measurements, and good agreement is observed for the evolved wave train.

Key words: Wave group evolution, wave breaking, High-Level Irrotational Green-Naghdi (HLIGN) equations, laboratory experiments

The wave breaking and the evolution of the wave groups are a critical topic in the investigation of extreme waves in deep water. The evolution of the non-breaking wave groups and the wave propagations in deep water are widely studied^[1-2]. Most of these studies suggest that the wave breaking should be further investigated.

Several experiments of the wave group evolution are conducted to investigate the wave breaking^[3-4]. However, a quantitative analysis of breaking waves in the modulated wave train with limited number of waves is yet to be achieved^[5]. This paper presents a further laboratory investigation of the wave breaking in regular wave trains.

The experiments are conducted in the fluid mechanics laboratory of Harbin Engineering University. A sketch of the wave flume is shown in Fig. 1. The wave flume is 25.0 m long and 2.0 m wide, with a fixed water depth of 1.0 m.

Plunger type wave generators move simultaneously in the vertical direction to generate regular

waves at one end of the tank. As seen in Eq. (1), the ramping time t_{ramp} is 3.0 s, which allows for a smooth transition from the still water position to the maximum oscillation position A_{\max} . The total operating time of the wave maker is t_{total} . On the other end of the tank, there is a multi-layer sponger-type wave absorber.

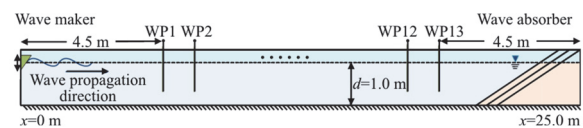


Fig. 1 (Color online) Sketch of the physical wave tank, as well as the locations of the first and last gauges. Not in real scale

$$A = A_{\max} \frac{t}{t_{\text{ramp}}}, \quad 0 < t \leq t_{\text{ramp}} \quad (1a)$$

$$A = A_{\max}, \quad t_{\text{ramp}} < t \leq t_{\text{total}} - t_{\text{ramp}} \quad (1b)$$

$$A = A_{\max} \frac{t_{\text{total}} - t}{t_{\text{ramp}}}, \quad t_{\text{total}} - t_{\text{ramp}} < t \leq t_{\text{total}} \quad (1c)$$

$$A = 0, \quad t_{\text{total}} < t \quad (1d)$$

Two experimental wave conditions listed in Table 1 are considered here. The wave steepness is the

Projects supported by the National Natural Science Foundation of China (Grant No. 11772099), the Heilongjiang Touyan Innovation Team Program, China.

Biography: Wen-yang Duan (1967-), Male, Ph. D., Professor, E-mail: duanwenyang@hrbeu.edu.cn

Corresponding author: Bin-bin Zhao,
E-mail: zhaobinbin@hrbeu.edu.cn

ratio of the initial wave height H to the wave length λ , which is calculated by the linear dispersion relation from the wave period T . The value of t_{total} affects the number of waves per packet (the lengths of the wave trains^[2]). A settling time of approximately 10 minutes between two successive measurements is to make the water in the tank become calm.

Table 1 Physical test cases

Case	T / s	H / m	$H \cdot \lambda^{-1}$	$t_{\text{total}} / \text{s}$
R1016-10	1.0	0.16	0.10	10
R1016-14	1.0	0.16	0.10	14

Thirteen capacitance type wave probes are placed in a line along the center of the wave flume. The probes record the time history of the surface elevation at the same time. The sampling frequency is 50 Hz. The location of each wave probe from the wave maker is listed in Table 2.

Table 2 Locations of wave probes, measured from the wave-maker end of the tank

No.	x / m
1	4.5
2	5.5
3	7.0
4	8.5
5	10.0
6	11.5
7	13.0
8	14.5
9	16.0
10	17.5
11	18.6
12	19.0
13	20.5

As an example, the breaking surface elevations at two moments in the cases R1016-10, R1016-14, respectively, are shown in Fig. 2. The waves propagate from left to right. The free surface between the two yellow lines is a breaking crest. The “white hat” on the breaking crest is chaotic in nature. There is another breaking wave occurred earlier before this breaking crest. As a result, the free surface after breaking is scattered. The wave breaking observed in our experiments occurs only at the preceding wave of the wave groups. And the behavior of the breaking crest is similar in the cases R1016-10, R1016-14. Each case in the laboratory experiments is repeatable, which will not all be shown here.

The time series of the surface elevation recorded by the 13 wave gauges are shown in Fig. 3. The black lines are the surface elevations, and the red lines indicate the upper envelopes to illustrate the evolution

of the wave train. The wave train envelope is not uniform even at the first wave probe ($x = 4.5 \text{ m}$) because of the strong nonlinearity. As indicated in Fig. 3, the wave breaking occurs at the place $x > 5.5 \text{ m}$ for the wave trains R1016-10, R1016-14, despite the fact that the packet lengths (in time) of them are different. And the asymmetric wave envelopes are observed in both cases. The wave train moves with a forward slope and the largest slope occurs on the preceding face of the wave envelope where the wave breaking is observed. The different packet length appears to affect the number of envelope peaks of the evolved wave train. As the wave breaking only occurs at the preceding wave of the wave groups, the geometric property in this region deserves to be further investigated.

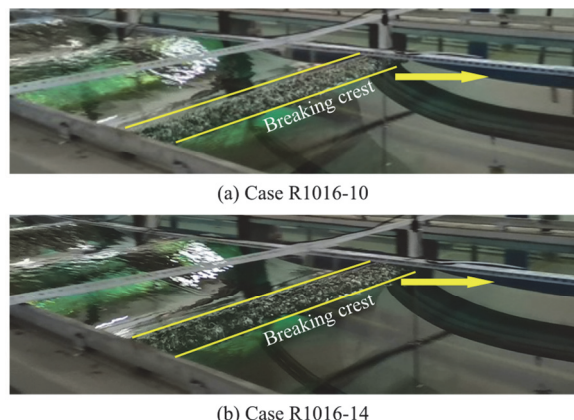


Fig. 2 (Color online) Photos of breaking moments

Figure 4 shows the evolution of some local geometric property near the maximum wave (η_{\max}) at the leading side of the measured time series approximately at the time of wave breaking. A local wave steepness ($\varepsilon_{\text{loc}} = k_1 \eta_{\max}$, where k_1 is the local wave number^[6]) indicates the nonlinearity of the maximum wave crest. A skewness parameter (S_k) indicates the correlation between the maximum crest and the adjacent troughs^[6]. The dashed line and the solid line are the measured data of the cases R1016-10, R1016-14.

Figure 4 shows that the measurements in both cases have the same tendency during the propagation despite of the different packet lengths. The wave breaking and the nonlinear modulation often lead to decreasing and increasing performances of these local geometric parameters, respectively. In Fig. 4(a), accompanied with the first wave breaking event near the wave-maker ($x > 5.5 \text{ m}$), the oscillatory behavior is observed for the local steepness around the breaking limitation ($k_1 \eta_{\max} = 0.45$ or $H / \lambda = 1/7$) for the

deep-water regular wave. The extreme values for the local steepness are 0.72, 0.71 for the cases R1016-10, R1016-14, respectively. By definition^[6], a positive skewness means that the maximum crest is larger than its nearby troughs. Figure 4(b) shows that S_k is positive at all wave gauges. At $x=19.0$ m in the case R1016-14, it even approaches 1.0, which means that η_{\max} is twice of the value at its nearby troughs.

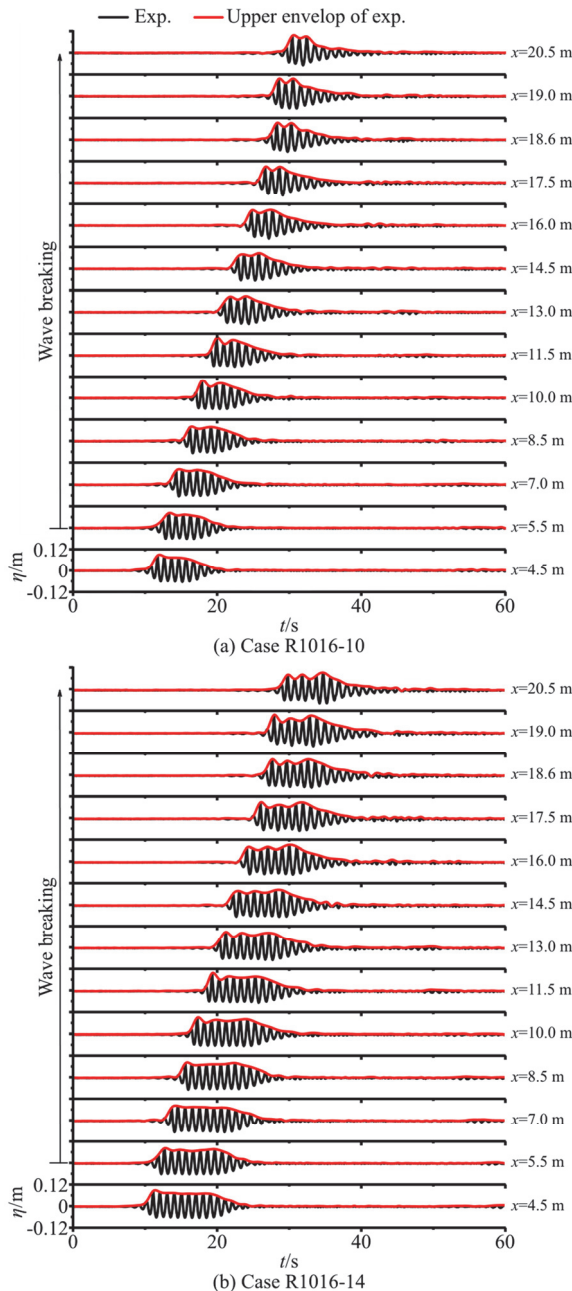


Fig. 3 (Color online) Evolution of wave surface elevation measured by the wave gauges in the wave flume

Some investigations focused on the prediction of the wave breaking. For the wave breaking in shallow

water near the coastal regions, the momentum conserved eddy viscosity model^[7] and the hybrid wave breaking model^[8] are usually utilized in the Boussinesq wave models^[9]. Barthelemy et al.^[10] introduced a robust threshold parameter for the breaking onset for 2-D wave packets propagating in the deep water and the intermediate depth water. For the deep-water breaking wave, the laboratory studies on breaking wave were carefully performed by Tian et al.^[11], and the result becomes a benchmark for the investigation of the wave breaking models. An eddy viscosity wave breaking model was proposed, which is widely used for various numerical investigations of wave breaking in deep water^[12].

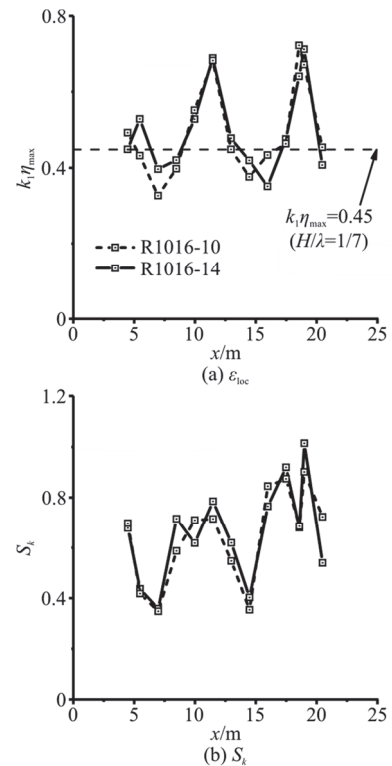


Fig. 4 Local geometric parameters near the maximum wave recorded by the 13 wave gauges

In this paper, the High Level Irrotational Green-Naghdi (HLGN) equations are utilized in the wave simulation, and the eddy viscosity wave breaking model^[11] is added into the HLGN equations to study the wave breaking characteristics in regular wave trains, which are also verified with the laboratory experiments mentioned above.

The fluid is assumed to be incompressible and inviscid and the flow is irrotational. The HLGN equations are derived based on the Hamilton's principle, the mass conservation equation and the momentum conservation equation (Euler equation). The fully non-linear boundary conditions are posed on the free surface.

In two dimensions, the origin of the coordinate system (x, z) is at the mean water level. The free surface elevation measured from the still-water level is specified by $z = \eta(x, t)$. The sea bottom is flat and stationary, $d(x) = -d$. The velocity field (u, w) can be expressed by the stream function $\Psi(x, z, t)$ as a series of polynomials with stream function coefficients $\Psi_n(x, t)$, as follows:

$$u = \frac{\partial \Psi(x, z, t)}{\partial z}, \quad w = -\frac{\partial \Psi(x, z, t)}{\partial x} \quad (2a)$$

$$\Psi(x, z, t) = \sum_{n=1}^K \psi_n(x, t) \gamma^{2n-1}, \quad K = 1, 2, 3, \dots \quad (2b)$$

where $\gamma = (z + d) / (\eta + d)$. This approximation of the wave kinematics could be improved to a higher level by increasing the order of the polynomials K . When compared to the perturbation-based approaches, it is demonstrated that the HLIGN equations represent a strongly nonlinear and strongly dispersive wave model.

As the HLIGN equations are well-introduced in previous papers, here we only give a brief introduction to the equations. The detailed expressions and explanations can be found in Ref. [13].

Tian et al.^[11] proposed an empirical eddy viscosity model to consider the energy dissipation due to the wave breaking. For the time-domain simulation of the breaking waves, the eddy viscosity dissipation is confined only to the moment and the space when and where the wave breaking occurs, otherwise, the fluid is inviscid throughout. We implement this model in the HLIGN equations, following Tian et al.^[11]. Determining the wave breaking criterion is the primary step of a breaking model. The wave breaking onset in Tian et al.^[11] is a local geometrical parameter, S , which is the local surface elevation slope defined as the spatial derivative of the surface elevation $S = \partial \eta / \partial x$. When the wave crests approach the breaking point, an eddy viscosity term will be activated to dissipate the energy due to the wave breaking. This eddy viscosity is adopted in the time derivatives of the free surface and the stream function coefficients to be solved in the HLIGN equations, as:

$$\frac{\partial \eta}{\partial t} = \frac{\partial \eta}{\partial t} + 2\nu_{\text{eddy}} \frac{\partial^2 \eta}{\partial x^2} \quad (3a)$$

$$\frac{\partial \psi_n}{\partial t} = \frac{\partial \psi_n}{\partial t} + 2\nu_{\text{eddy}} \frac{\partial^2 \psi_n}{\partial x^2}, \quad n = 1, 2, \dots, K \quad (3b)$$

where the eddy viscosity ν_{eddy} is expressed by

$$\nu_{\text{eddy}} = \alpha \frac{H_{br} L_{br}}{T_{br}} \quad (3c)$$

where $\alpha = 0.02$, as recommended by Tian et al.^[11]. Details about the horizontal breaking length L_{br} , the breaking time T_{br} and the falling crest height H_{br} can be found in Ref. [11].

The numerical simulations are performed by use of the HLIGN equations with the wave breaking model for the same cases as in the laboratory experiments. All simulations are performed in the time domain. The converged spatial grid size is $dx = \lambda / 50$, the time step is $dt = dx / 2c$, where c is the phase speed of the initial regular waves. The converged level of the HLIGN equations is 5. To reduce the effect of reflections, the length of the numerical wave absorber is 3.0 m, nearly twice of the wavelength of the initial regular wave.

Figure 5 shows the comparisons between the HLIGN results and the experimental data obtained from three wave probes, $x = 4.5$ m, 11.5 m and 18.6 m, where the distance between two adjacent wave probes is about 7.0 m. This distance is long enough to observe any difference for the evolving time history of the wave envelope. Excellent agreement is found between the results of the HLIGN equations and the laboratory data, although the wave breaking poses a great challenge to predict the exact surface elevation of the evolving wave groups.

Figure 6 shows the estimated time integration of the surface elevation $\langle \eta^2 \rangle$, which is proportional to the potential energy^[11], for each wave probe, illustrating the energy dissipation during the propagation. The black square dots and the solid line represent the experimental data and its fitting line obtained by the least square method. The red circular dots are the calculation results based on the HLIGN results.

Significant energy dissipation is observed along the wave tank, as shown in Fig. 6. The wave breaking continuously occurs over the tank length, along with the continuous reduction of the energy. The slope of the fitting line is nearly identical in these two cases. It approaches 1.30×10^{-4} , 1.32×10^{-4} , in the cases R1016-10, R1016-14, respectively. The energy dissipation between two wave probes at a distance of nearly 10λ (from $x = 4.5$ m to $x = 20.5$ m) could be determined as $(\langle \eta^2 \rangle_{x=4.5 \text{ m}} - \langle \eta^2 \rangle_{x=20.5 \text{ m}}) / (H^2 T)$. Owing to the significant wave breaking, the dissipation can reach 12.3%, 11.3% for R1016-10, R1016-14, respectively. Again, the numerical results agree very well with the laboratory measurements and their fitting lines.

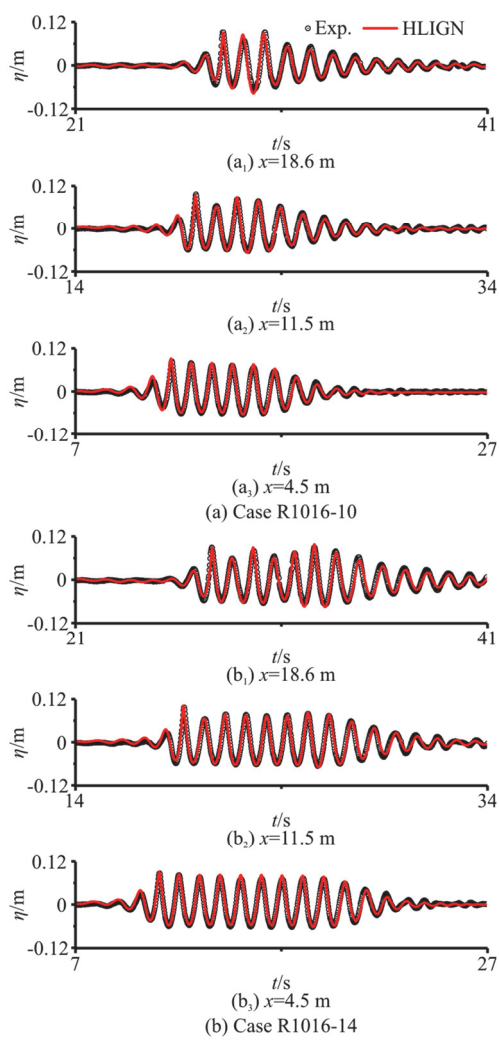


Fig. 5 (Color online) Comparison of time series measured by the wave gauges, in laboratory (dot), and calculated by the HLIGN model (line)

In this paper, the evolution of the strongly nonlinear deep-water gravity wave groups with wave breaking is studied by conducting laboratory experiments and performing numerical simulation. Conclusions are as follows:

(1) In the experiments, the evolving wave train moves with a forward slope and the largest slope occurs on the preceding face of the asymmetric wave envelope, where wave breaking is observed. In our experiment, we consider two wave trains with different packet lengths (R1016-10, R1016-14). The behaviour of them is quite similar with respect to the effect of the wave breaking. Some local geometric property appears to be oscillatory during the wave evolution affected by the wave breaking. Extreme values of the local steepness and skewness are nearly 0.7 and 1.0, respectively. Continuous decreasing tendency of the energy is observed during the propagation of the breaking wave train. From $x = 4.5$ m to

$x = 20.5$ m, nearly a distance of 10λ , the energy dissipation can reach 12.3% due to the significant wave breaking.

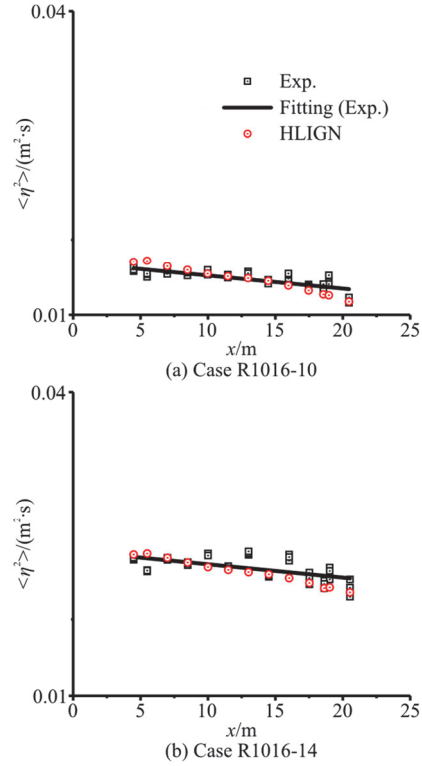


Fig. 6 (Color online) Comparison of energy dissipation based on the laboratory measurements and the HLIGN calculations

(2) The wave breaking model based on an empirical eddy viscosity approximation^[11] is implemented into the HLIGN equations to consider the wave breaking effects. Good agreement is observed between the results of the HLIGN equations with the wave breaking model, and the laboratory measurements.

References

- [1] Feir J. E. Discussion: some results from wave pulse experiments [J]. *Proceedings of the Royal Society of London. Series A. Mathematical and Physical Sciences*, 1967, 299 (1456): 54-58.
- [2] Zheng K., Zhao B. B., Duan W. Y. et al. Simulation of evolution of gravity wave groups with moderate steepness [J]. *Ocean Modelling*, 2016, 98: 1-11.
- [3] Su M. Y. Evolution of groups of gravity waves with moderate to high steepness [J]. *Physics of Fluids*, 1982, 25(12): 2167-2174.
- [4] Liang S. X., Sun Z. C., Chang Y. L. et al. Evolution characteristics and quantization of wave period variation for breaking waves [J]. *Journal of Hydrodynamics*, 2020, 32(2): 361-374.
- [5] Zheng K., Zhao B. B., Duan W. Y. Experimental study on

- wave breaking and evolution of wave groups with high steepness [C]. *The 37th International Workshop on Water Waves and Floating Bodies*, Giardini Naxos, Italy, 2022.
- [6] He Y. L., Ma Y. X., Ma X. Z. et al. Experimental analysis of the nonlinear evolution of single wave group in deep water [J]. *Journal of Harbin Engineering University*, 2019, 40(11): 1839-1845.
 - [7] Kennedy A. B., Chen Q., Kirby J. T. et al. Boussinesq modeling of wave transformation, breaking, and runup. I: 1D [J]. *Journal of Waterway, Port, Coastal, and Ocean Engineering*, 2000, 126(1): 39-47.
 - [8] Shi F., Kirby J. T., Harris J. C. et al. A high-order adaptive time-stepping TVD solver for Boussinesq modeling of breaking waves and coastal inundation [J]. *Ocean Modelling*, 2012, 43: 36-51.
 - [9] Kazolea M., Ricchiuto M. On wave breaking for Boussinesq-type models [J]. *Ocean Modelling*, 2018, 123: 16-39.
 - [10] Barthelemy X., Banner M. L., Peirson W. L. et al. On a unified breaking onset threshold for gravity waves in deep and intermediate depth water [J]. *Journal of Fluid Mechanics*, 2018, 841: 463-488.
 - [11] Tian Z., Perlin M., Choi W. Y. An eddy viscosity model for two-dimensional breaking waves and its validation with laboratory experiments [J]. *Physics of Fluids*, 2012, 24(3): 036601.
 - [12] Liu S., Zhang X. S. Extreme wave crest distribution by direct numerical simulations of long-crested nonlinear wave fields [J]. *Applied Ocean Research*, 2019, 86: 141-153.
 - [13] Zhao B. B., Zheng K., Duan W. Y. et al. Time domain simulation of focused waves by High-Level Irrotational Green-Naghdi equations and Harmonic Polynomial Cell method [J]. *European Journal of Mechanics-B/Fluids*, 2020, 82: 83-92.